Radar altimetry backscattering signatures at Ka, Ku, C, and S bands over West Africa

Frédéric Frappart, C. Fatras, Éric Mougin, V. Marieu, A.T. Diepkilé, F. Blarel, P. Borderies

▶ **To cite this version:**

Frédéric Frappart, C. Fatras, Éric Mougin, V. Marieu, A.T. Diepkilé, et al.. Radar altimetry backscattering signatures at Ka, Ku, C, and S bands over West Africa. Physics and Chemistry of the Earth. Parts A/B/C, 2015, 83-84, pp.96-110. 10.1016/j.pce.2015.05.001 . hal-01414511

HAL Id: hal-01414511
https://hal.science/hal-01414511

Submitted on 4 Oct 2021

HAL is a multi-disciplinary open access archive for the deposit and dissemination of scientific research documents, whether they are published or not. The documents may come from teaching and research institutions in France or abroad, or from public or private research centers.

L'archive ouverte pluridisciplinaire **HAL**, est destinée au dépôt et à la diffusion de documents scientifiques de niveau recherche, publiés ou non, émanant des établissements d'enseignement et de recherche français ou étrangers, des laboratoires publics ou privés.

Distributed under a Creative Commons Attribution 4.0 International License

Radar altimetry backscattering signatures at Ka, Ku, C, and S bands over West Africa

F. Frappart [a,b,*], C. Fatras [a,c], E. Mougin [a], V. Marieu [d], A.T. Diepkilé [e], F. Blarel [b], P. Borderies [c]

[a] GET-GRGS, UMR 5563, CNRS/IRD/Université de Toulouse, Observatoire Midi-Pyrénées, 14 Avenue Edouard Belin, 31400 Toulouse, France
[b] LEGOS-GRGS, UMR 5566, CNES/CNRS/IRD/Université de Toulouse, Observatoire Midi-Pyrénées, 14 Avenue Edouard Belin, 31400 Toulouse, France
[c] ONERA, 2 Avenue Édouard Belin, 31055 Toulouse Cedex 4, France
[d] EPOC-OASU, UMR 5805, Allée Geoffroy St Hilaire, 33615 Pessac Cedex, France
[e] LOSSA–USTTB/Université des Sciences, des Techniques et des Technologies de Bamako, Mali

This study presents a comprehensive comparison of radar altimetry signatures at Ka-, Ku-, C-, and S-bands using SARAL, ENVISAT and Jason-2 data over the major bioclimatic zones, soil and vegetation types encountered in West-Africa, with an emphasis on the new information at Ka-band provided by the recently launched SARAL–Altika mission. Spatio-temporal variations of the radar altimetry responses were related to changes in surface roughness, land cover and soil wetness. Analysis of time series of backscattering coefficients along the West African bioclimatic gradient shows that radar echoes at nadir incidence are well correlated to soil moisture in semi-arid savannah environments. Radar altimeters are able to detect the presence of water even under a dense canopy cover at all frequencies. But only measurements at Ka-band are able to penetrate underneath the canopy of non-inundated tropical evergreen forests.

1. Introduction

Spaceborne radar sensors provide global observation of continental surfaces at different frequencies, resolution, incidence angles and polarizations. Backscattering coefficients (σ_0) from radar scatterometers and Synthetic Aperture Radar (SAR) images are commonly used to monitor the dynamics of key variables characterizing the continental surfaces, such as vegetation density or surface soil moisture. Over West Africa, side-looking radar scatterometers, notably the C-band wind-scatterometer (WSC) onboard the European Remote Sensing satellites ERS-1 (launched in 1991) and ERS-2 (launched in 1995), already demonstrated a strong potential for the monitoring of surface dielectric properties (Mougin et al., 1995; Frison and Mougin, 1996a) related to soil moisture changes (Wagner et al., 1999a; Naeimi et al., 2009; Zribi et al., 2009) and vegetation dynamics (Frison and Mougin, 1996b, 1998; Hardin et al., 1996; Wagner et al., 1999b; Woodhouse and Hoekman, 2000) at a spatial resolution of approximately 50 km. In addition, SAR images were widely used to map the temporal variation of surface soil moisture (SSM) over semi-arid environments such as Sahelian savannahs (Baup et al., 2007, 2011; Zribi et al., 2006), land cover (Simard et al., 2001; Mayaux et al., 2002), and wetland extents along the hydrological cycle (van de Giesen, 2001; Rosenqvist and Birkett, 2002; Betbeder et al., 2014) at C and L bands, for spatial resolutions lower than one kilometer and temporal resolution greater than 1 month.

Spatial and temporal variations of radar altimeter (RA) backscattering coefficients were related to the dynamics of surface properties. Signatures of soil roughness and SSM changes in the Sahara desert were identified using ERS-1 data at Ku band (Cudlip et al., 1994). Backscattering coefficients from Topex/Poseidon were found to be decreasing as vegetation increase in Sahel (Prigent et al., 2014). A comprehensive comparison of radar signatures acquired over West Africa (between 0–25°N and 5°W–25°E) at both C- and Ku-bands using nadir-looking altimeters (35-day orbital period ENVISAT RA-2 over 2003–2010 and 10-day orbital period Jason-2 over mid-2008–2012) that covers the major bioclimatic zones, soil and vegetation types encountered in this region was performed (Fatras et al., 2015). A recent study also demonstrated the capability to retrieve SSM from ENVISAT RA-2 backscattering coefficients over Sahelian savannahs in the Gourma region of Mali (Fatras et al., 2012).

* Corresponding author at: LEGOS-GRGS, UMR 5566, CNES/CNRS/IRD/Université de Toulouse, Observatoire Midi-Pyrénées, 14 Avenue Edouard Belin, 31400 Toulouse, France. Tel.: +33 (0) 5 61 33 30 95; fax: +33 (0) 5 61 33 25 60.
E-mail address: frederic.frappart@get.obs-mip.fr (F. Frappart).

In this study, we analyzed the backscattering signatures at Ka-band from AltiKa, the first altimeter to operate at this frequency band, onboard SARAL (Vincent et al., 2006; Verron et al., in press), along with the ones at Ku- and C-bands from Jason-2 and at Ku- and S-bands from ENVISAT, for representative areas of the bioclimatic conditions present in West Africa. For the very first time, temporal variations of the radar altimetry responses at Ka-band were studied over nine representative sites of the West African bioclimatic gradient along the altimeter tracks crossing the wetland region of the Inner Niger Delta, and compared to the radar altimetry signatures from current (Jason-2) and previous (ENVISAT) missions. Our goal is to examine how the spatio-temporal variations of the surface properties, related to soil roughness, water content (i.e., SSM or presence of open water), and vegetation cover, impact the radar responses of land surfaces in the different frequency bands.

2. Study area and datasets

2.1. Study area

West Africa (between latitudes 0–25°N and longitudes 5°W–25°E) exhibits a wide range of bioclimatic conditions from desert areas in the north, semi-arid savannahs under Sahelian and Soudanian climates, to wet tropical areas in the south. The duration of the rainy season, as well as the annual total rainfall, increase from north to south along the bioclimatic gradient (Nicholson, 1980; Le Barbé et al., 2002), as well as the vegetation cover and density. Nine study sites were selected, distributed in the main ecoclimatic zones of West Africa: two in the Sahara (stone and sand desert sites); four in savannah landscapes, at the transition between the Sahara and Sahel (Saharo–Sahelian site), in Sahel (Sahelian site), at the transition between the Soudanian and Sahelian zones (Soudano-Sahelian site), in the Soudanian region (Soudanian site); one in the inner delta of the Niger River, and finally two in humid tropical forests over non and temporarily flooded areas (Fig. 1 and Table 1). Two sub-sites are associated to each study site, corresponding to the location of the altimeter tracks from ENVISAT and SARAL on the one hand, and Jason-2 on the other hand. They are chosen to be as close as possible to each other.

The stone desert sites in the Libyan part of the Sahara are flat areas of Nubian sandstone with small roughness and almost constant climate, since the Libyan Desert is known for being one of the driest parts of the world (Isnard, 1968). The sandy desert sites in the Ténéré region of Niger consist of sand dunes and are subject to almost no rainfall throughout the year. Savannah sites correspond to landscapes with gently undulating sandy dunes and a moderate roughness. They are affected by the West African

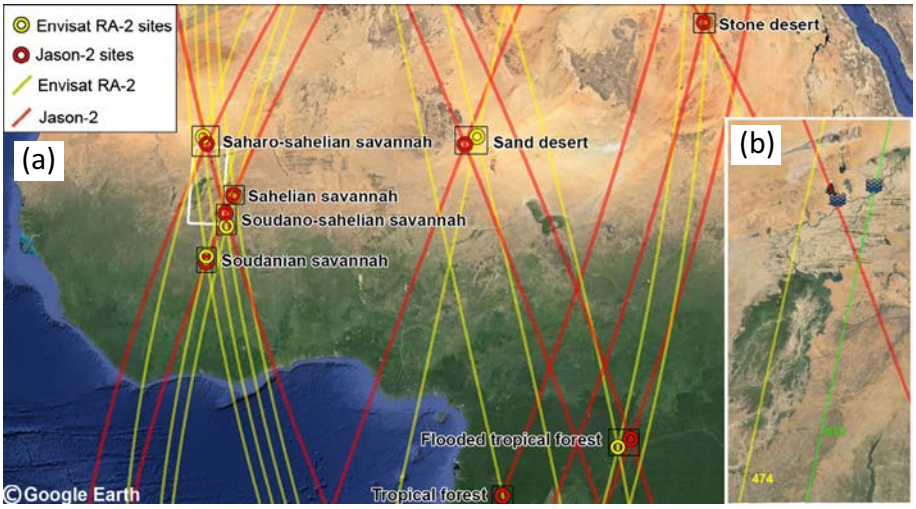

Fig. 1. Location of study sites under radar altimetry tracks over West Africa (between 0–25°N and 5°W–25°E). (a) Jason-2 (ENVISAT/SARAL) tracks used in this study are represented with red (yellow) lines, respectively. The corresponding study sites are represented with red and yellow circles, respectively. The white rectangle delineates the Inner Niger Delta in Mali. (b) Zoom in the Niger Inner Delta region. Spatio-temporal variations of the backscattering coefficients were analyzed along ENVISAT/SARAL track 0474 (yellow) and Jason-2 track 046 (red) and time series of water levels were derived at the intersections of ENVISAT/SARAL track 0932 (green) and Jason-2 track 046 (red), close to the gauge stations (black and blue checked pattern) of Diré and Tonka respectively. (For interpretation of the references to color in this figure legend, the reader is referred to the web version of this article.)

Table 1
Locations of the West African study sites under SARAL (Ka-band)/ENVISAT (Ku and S bands) Jason-2 (Ku and C bands) tracks.

Sites	SARAL (Ka) and ENVISAT (Ku and S)			Jason-2 (Ku and C)		
	Lon (°)	Lat (°)	Tracks	Lon (°)	Lat (°)	Tracks
Saharian Stone desert	24.2125	23.8453	0386/0743	24.0906	23.8453	007/120
Saharian Sand desert	10.5610	17.5614	0143/0616	9.9183	17.1743	172/211
Saharo–Sahelian savannah	−4.5283	17.5583	0016/0545	−4.2542	17.1763	046/085
Sahelian savannah	−2.3738	14.4672	0459/0846	−2.4740	14.5080	161
Soudano-Sahelian savannah	−2.7327	12.8978	0001/0846	−2.8368	13.5688	046/161
Soudanian savannah	−3.8099	11.3086	0087/0388	−3.8096	11.0040	161
Non flooded tropical evergreen forest	11.8037	−0.7940	0315	11.7609	−0.7940	020
Temporarily flooded tropical evergreen forest	17.7466	1.5932	429/472	18.4222	1.9884	083/248
Inner Niger Delta transect	−4.85/−3.90	14/17	0474	−4.20/−2.65	14/17	046
Inner Niger Delta virtual stations	−3.4115	16.1965	0932	−3.8049	16.0512	046

Monsoon (WAM), characterized by a single rainy season with most precipitation falling between late June and mid September (Nicholson, 1980; Le Barbé et al., 2002). The vegetation is composed of annual plants, mostly grasses with scattered bushes and low trees (Mougin et al., 2009). The Niger inner delta is a large floodplain located in central Mali, within the Sahelian zone between latitudes 13–17°N and longitudes 3–5°W. The extent of the flooded delta itself changes every year as a function of the intensity of the West African Monsoon and can be larger than 32,000 km^2 during the wettest rainy seasons (Zwarts and Grigoras, 2005; Jones et al., 2009). The flooding period extends from August to December and during the dry season, from March to May, the area dries out at the exception of the river bed and permanent lakes. The evergreen humid tropical forest sites are located in the Congo basin. They are characterized by a very high vegetation density showing almost no variation throughout the year due to quasi permanent moist conditions. One of them is subject to seasonal floods, the other not.

2.2. Radar altimetry data

2.2.1. SARAL

SARAL is a CNES-ISRO joint-mission that was launched on February 25th 2013. Its payload is composed of the AltiKa radar altimeter and bi-frequency radiometer, and a triple system for precise orbit determination: the real-time tracking system DIODE of DORIS instrument, a Laser Retroflector Array (LRA), and the Advanced Research and Global Observation Satellite (ARGOS-3). SARAL orbits at an average altitude of 790 km, with an inclination of 98.54°, on a sun-synchronous orbit with a 35-day repeat cycle. It provides observations of the Earth surface (ocean and land) from 82.4° latitude North to 82.4° latitude South. This orbit was formerly used by ERS-1 and 2 and ENVISAT missions, with an equatorial ground-track spacing of about 85 km. The first four cycles of SARAL do not follow precisely the ENVISAT orbit. AltiKa radar altimeter is a solid-state mono-frequency altimeter that provides accurate range measurements. It is the first altimeter to operate at Ka-band (35.75 GHz). Its accuracy is expected to be about 1 cm over ocean. Over the rivers, it is expected to provide measurements significantly better than those gained by the previous Ku band missions. Improvements come in the one hand from a reduced footprint in Ka band, about ten times smaller in surface than it is in the Ku band, and in the other hand from an along-track sampling at 40 Hz, twice that of ENVISAT and Jason-2.

2.2.2. ENVISAT

ENVISAT mission was launched on March 1st 2002 by ESA. It carried 10 instruments including the advanced radar altimeter (RA-2). It was based on the heritage of sensor on-board the European Remote Sensing (ERS-1 and 2) satellites. RA-2 was a nadir-looking pulse-limited radar altimeter operating at two frequencies at Ku- (13.575 GHz), as ERS-1 and 2, and S- (3.2 GHz) bands. Its goal was to collect radar altimetry over ocean, land and ice caps (Zelli, 1999). ENVISAT remained on its nominal orbit until October 2010 and its mission ended April 8th 2012. Its initial orbital characteristics are the same as for SARAL (see above).

2.2.3. Jason-2

Jason-2 mission was launched on June 20th 2008 as cooperation between CNES, EUMETSAT, NASA and NOAA. Its payload is mostly composed of the Poseidon-3 radar altimeter from CNES, the Advanced Microwave Radiometer (AMR) from JPL/NASA, and a triple system for precise orbit determination: the real-time tracking system DIODE of DORIS instrument from CNES, a GNSS receiver and a Laser Retroflector Array (LRA) from NASA. Jason-2 orbits at an altitude of 1336 km, with an inclination of 66°, on a 10-day repeat cycle, providing observations of the Earth surface (ocean and land) from 66° latitude North to 66° latitude South, with an equatorial ground-track spacing of about 315 km. This orbit was formerly used by Topex/Poseidon, and Jason-1. Poseidon-3 radar altimeter is a two-frequency solid-state altimeter that measures accurately the distance between the satellite and the surface (range) and provides ionospheric corrections over the ocean. It operates at Ku (13.575 GHz) and C (5.3 GHz) bands. Its accuracy is expected to be about 2 cm over ocean. Raw data are processed by SSALTO (Segment Sol multimissions d'ALTimétrie, d'Orbitographie).

All altimetry data used in this study come from the Geophysical Data Records (GDRs) – GDR T patch 2 for SARAL, GDR v2 for ENVISAT, GDR D for Jason-2, made available by Centre de Topographie de l'Océan et de l'Hydrosphère (CTOH – http://ctoh.legos.obs-mip.fr/). They are sampled along the altimeter track at 18, 20 and 40 Hz for ENVISAT, Jason-2 and SARAL respectively (high-frequency mode commonly used over land and coastal areas were the surface properties are changing more rapidly than over the open ocean). They consist of:

(i) the satellitelocations and acquisition times,
(ii) the corresponding backscattering coefficients at Ka band for SARAL (cycles 1–16 from February 2013 to August 2014), at Ku (cycles 6–94 from June 2002 to October 2010) and S (cycles 6–64 from June 2002 to January 2008 when RA-2 altimeter onboard ENVISAT stopped operating correctly at S-band) bands for ENVISAT, at Ku and C bands for Jason-2 (cycles 19–91 from January 2009 to December 2010 and cycles 168–227 from February 2013 to August 2014),
(iii) all the parameters necessary to estimate the altimeter heights (see Section 3.3 Time-variations of altimetry-based water levels in the Niger Inner Delta).

In the followings, ranges used to derive altimeter heights and backscattering coefficients are the ones processed with the Ice-1 retracking algorithm (Wingham et al., 1986). Previous studies showed that Ice-1-derived altimetry heights are the more suitable for hydrological studies in terms of accuracy of water levels and availability of the data (e.g., Frappart et al., 2006a,b; Santos da Silva et al., 2010) among the commonly available retracked data present in the GDRs. They were also used in previous studies for characterizing land surfaces properties (Fatras et al., 2012, 2015), showing a strong linear relationship with SSM (Fatras et al., 2012). Besides, they are present in the SARAL, ENVISAT and Jason-2 GDRs in the high-frequency mode.

2.3. Ancillary data

2.3.1. TRMM rainfall

The Tropical Rainfall Measuring Mission (TRMM) Multi-satellite (a Japan–US satellite launched in November 1997) Precipitation Analysis (TMPA) 3B42 v7 daily rainfall data, with a spatial resolution of $0.25° \times 0.25°$, are used from January 2003 to December 2011. This dataset is produced by combining several data products (Huffman et al., 2007, 2010):

(i) satellite information from the TRMM High Quality (HQ) combined microwave precipitation estimates reprocessed from the TRMM Combined Instrument (TCI), the TRMM Microwave Imager (TMI), Special Sensor Microwave/Imager (SSM/I), Advanced Microwave Scanning Radiometer for EOS (AMSR-E) on-board EOS Aqua, and the Advanced Microwave Sounding Unit B (AMSU- B) onboard the National Oceanic and Atmospheric Administration (NOAA KLM) satellites, with additional satellite data including the

early part of the Microwave Humidity Sounder (MHS) record, the entire operational Special Sensor Microwave Imager/Sounder (SSMIS) record (Huffman et al., 2010);

(ii) a new infrared (IR) brightness temperature data set from geosynchronous satellites for the period before the start of the Climate Prediction Center (CPC) 4-km Merged Global IR data set (January 1998–February 2000);

(iii) Global Precipitation Climatology Centre (GPCC) gauge analyses (Schneider et al., 2011). It is available on the Goddard Earth Sciences Data and Information Services Center (GES DISC) website: http://daac.gscf.nasa.gov.

2.3.2. AMSR-E soil moisture

The Advanced Microwave Scanning Radiometer (AMSR-E) from the Japanese space agency onboard the Aqua (EOS PM-1) satellite is dedicated to the observation of climate and hydrology. It is a multi-frequency dual-polarized microwave radiometer operating at C- and X-bands that detects faint microwave emissions from the Earth's surface and atmosphere. The VUA-NASA Land Retriever Parameter Model (LPRM) is a forward radiative transfer model that used passive microwave remote sensing data to retrieve SSM (Owe et al., 2008). Available products cover the period June 2002–October 2011. In this study, we only consider C-band level 3 LPRM VUA (Vrije Universiteit of Amsterdam) products, which are available online (http://www.falw.vu/~jeur/lprm/) for the descending orbit, corresponding to night-time measurements (equator crossing time: 1:30 am) at a spatial resolution of $0.25^\circ \times 0.25^\circ$.

2.3.3. SMOS soil moisture

The Microwave Imaging Radiometer with Aperture Synthesis (MIRAS) sensor onboard the Soil Moisture and Ocean Salinity (SMOS) records satellite brightness temperatures at L-band (1.4 GHz) since January 2010. SSM estimates are obtained using an iterative inversion approach of the multi-angular observations of the brightness temperatures (Wigneron et al., 2007; Kerr et al., 2012).

The SMOS products used in this study are the Level 3 Soil Moisture (L3SM) products from the CNES CATDS (Centre Aval de Traitement des Données SMOS) from February 2013 to August 2014. They are daily available in the EASE (Equal Area Scalable Earth) grid format with a spatial resolution of 25 km. The version of the products used is the 2.7.1.

2.3.4. In-situ water levels

Records from the Diré, located at 3.383°W of longitude and 16.267°N of latitude, and Tonka, located at 3.75°W of longitude and 16.127°N of latitude, gauge stations were provided by the Malian hydrological service, Direction Nationale de l'Hydraulique (DNH). In this study, we used the time series of water levels from February 2013 to September 2014 for the Diré gauge station and from January 2009 to December 2010 for the Tonka gauge station.

3. Methods

3.1. Time-variations of σ_0 over specific sites

For each of the specific site presented in Section 2.1, backscattering coefficients were edited using a 3-sigma criterion and along-track averaged over distance of plus or minus 2.5 km from altimeter tracks crossings (see Table 1) using Eqs. (1) and (2):

$$\langle \sigma_0 \rangle_{dB} = 10\log_{10}(\langle 10^{\sigma_0/10} \rangle) \quad (1)$$

$$std(\sigma_0)_{dB} = 10\log_{10}\left(1 + \frac{std(10^{\sigma_0/10})}{\langle 10^{\sigma_0/10} \rangle}\right) \quad (2)$$

where $\langle \sigma_0 \rangle_{dB}$ and $\mathrm{std}(\sigma_0)_{dB}$ stand for the average of σ_0 in dB and its associated standard deviation in dB, respectively. As the backscattering coefficients of the different altimetry missions are provided in dB in the GDRs, they were first converted into their natural values as expressed in Eqs. (1) and (2).

Time-series of backscattering coefficients were obtained from February 2013 to August 2014 for SARAL at Ka-band and Jason-2 at C and Ku bands, and from June 2002 to October 2010 and June 2002 to January 2008 for ENVISAT at Ku and S bands respectively.

3.2. Spatio-temporal variations of σ_0 in the Niger Inner Delta

Backscattering coefficients are along-track averaged for each satellite pass at a spatial resolution of 0.008° (~1 km) over the Niger Inner Delta, between 13° and 17°N, using Eq. (1). Spatio-temporal variations of σ_0 are presented using Hovmoller diagrams showing variations of σ_0 at the different frequency bands plotted for time and latitude (see Section 4.2 Spatio-temporal variations of backscattering along the meridian transects). The corresponding longitudes can be inferred from Fig. 1b from the latitude and the altimetry track number.

3.3. Time variations of altimetry-based water levels in the Niger Inner Delta

For water studies over land, radar altimeter derived water levels have been shown to be precise enough and are now used for systematic monitoring of large rivers, lakes, wetlands and floodplains (e.g., Birkett, 1995, 1998; Frappart et al., 2005, 2012; Santos da Silva et al., 2010; Crétaux et al., 2011; Goita and Diepkile, 2012).

The principle of radar altimetry is the following: the altimeter emits a radar pulse and measures the two-way travel-time from the satellite to the surface. The distance between the satellite and the Earth surface – the altimeter range (R) – is thus derived with a precision of a few centimeters. The satellite altitude (H) referred to an ellipsoid is known from orbitography modeling with an accuracy better than 2 cm. Taking into account propagation corrections caused by delays due to interactions of electromagnetic wave in the atmosphere, and geophysical corrections, the height of the reflecting surface (h) with reference to an ellipsoid can be estimated as:

$$h = H - \left(R + \sum \Delta R_{propagation} + \sum \Delta R_{geophysical}\right) \quad (3)$$

where H is the height of the center of mass of the satellite above the ellipsoid from precise orbit determination (POD) technique, R is the nadir altimeter range from the center of mass of the satellite to the sea surface, $\sum \Delta R_{propagation}$ and $\sum \Delta R_{geophysical}$ are the sums of the geophysical and environmental corrections to apply to the range and respectively given by Eqs. (4) and (5):

$$\sum \Delta R_{propagation} = \Delta R_{ion} + \Delta R_{dry} + \Delta R_{wet} \quad (4)$$

ΔR_{ion} is the atmospheric refraction range delay due to the free electron content associated with the dielectric properties of the ionosphere, ΔR_{dry} is the atmospheric refraction range delay due to the dry gas component of the troposphere, and ΔR_{wet} is the atmospheric refraction range delay due to the water vapor and the cloud liquid water content of the troposphere,

$$\sum \Delta R_{geophysical} = \Delta R_{solid\ Earth} + \Delta R_{pole} \quad (5)$$

where $\Delta R_{solid\ Earth}$ and ΔR_{pole} are the corrections respectively accounting for crustal vertical motions due to the solid Earth and

pole tides. The propagation corrections applied to the range are derived from the Global Ionospheric Maps (GIM) and Era Interim model outputs from the European Centre Medium-Range Weather Forecasts (ECMWF) for the ionosphere and the dry and wet troposphere range delays respectively.

A virtual station is defined as a given intersection of an orbit groundtrack and a water body (i.e., lake, reservoir river channel, floodplain or wetland). There, the variations of the altimeter height h from one cycle to the other can be associated to changes in water level.

In this study, we used the Multi-mission Altimetry Processing Software (MAPS) that allows a refined selection of the valid altimetry data to build virtual stations (Frappart et al., in press) in the Inner Niger Delta. Data processing is composed of three main steps: a coarse delineation of the virtual stations using Google Earth, a refined selection of the valid altimetry data, and a computation of the water level time-series. The altimetry-based water level is computed for each cycle using the median of the selected altimetry heights, along with their respective deviation (i.e., mean absolute deviations) after correction of off-nadir effect. Parabolic profiles caused by non-nadir reflections (i.e., hooking effect) affecting part of the along-track observations are corrected as follows:

$$h(s_0) = h(s_i) + \frac{1}{2R(s_0)}\left(1 + \left(\frac{\partial H}{\partial s}(s_i)\right)^2\right)(ds)^2 \quad (6)$$

where s is the along-track coordinate, $h(s_0)$ is the altimeter height at nadir, $R_{corr}(s_0)$ the altimeter range at nadir corrected from the geophysical and environmental effects, s_0 the location of the nadir along the altimeter track, s_i the coordinates of the slant measurements, $\partial H/\partial s$ the rate of altitude variation of the satellite along the orbital segment, ds the along track difference between s_0 and s_i.

The altimeter height at nadir is obtained by estimating the summit of the parabola representing the actual water level:

$$h(s_0) = as_0^2 + bs_0 + c \quad (7)$$

where a, b and c are the coefficients of the parabola estimating through a least-square fitting of the altimeter data affected by hooking. See Santos da Silva et al. (2010) for more details.

This process is repeated each cycle to construct the water level time series at the virtual stations.

4. Results

4.1. Times series analysis over the study sites

4.1.1. Stone desert

Altimetry backscattered responses over stone deserts are quite stable (std < 1.5 dB) for every frequency (Fig. 2). Their average values decrease from ~27 dB at S-band to ~9 dB at Ka-band as the frequency increase. The difference in backscattering is ~7 dB between C and Ku bands using Jason-2 data and ~5–6 dB between S and Ku bands using ENVISAT data (Tables 2 and 3). Variations of amplitude from 2 to 4 dB with higher values during summer 2014 can be observed at Ka-band using SARAL measurements.

4.1.2. Sand desert

As over stone deserts, σ_0 values from radar altimetry are quite stable (std < 2 dB) for every frequency over sand deserts (Fig. 3). Their average values are lower than over stone deserts varying

Table 2
Mean and standard deviation (Std) of the backscattering coefficients from SARAL (Ka-band), ENVISAT (Ku and S bands), estimated from February 2013 to August 2014, and from June 2002 to October 2010 respectively, over the West African study sites showing temporal stable radar responses. – : No SARAL data were available over the Saharian stone desert site for track 0386.

Sites	Track	SARAL (Ka)		ENVISAT (Ku)		ENVISAT (S)	
		Mean (dB)	Std (dB)	Mean (dB)	Std (dB)	Mean (dB)	Std (dB)
Saharian stone desert	0386	–	–	21.17	0.65	26.63	1.01
	0743	9.05	1.46	21.70	0.84	27.59	0.96
Saharian sand desert	0143	4.90	1.65	9.64	1.39	13.37	0.42
	0616	4.27	1.12	9.77	1.18	13.30	0.35
Non flooded tropical evergreen forest	0315	16.93	2.94	13.93	3.79	13.50	4.50

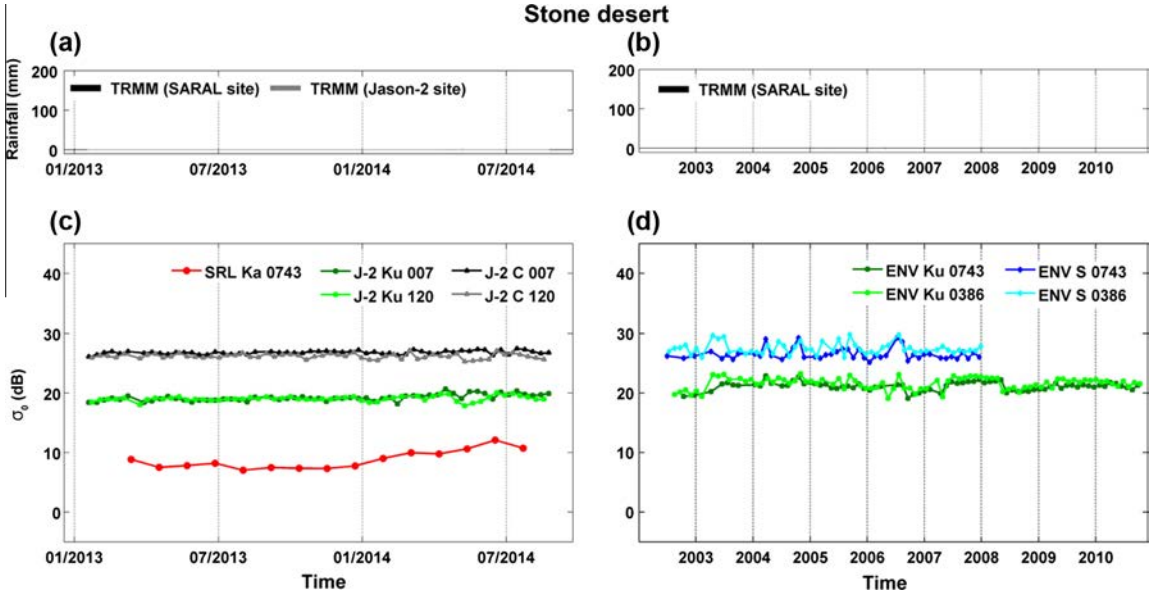

Fig. 2. Time series of daily rainfall (mm) from TRMM 3B423 v7 at (a) SARAL (black) and Jason-2 (gray) sites, (b) ENVISAT site (black). Time series of backscattering coefficient (dB) for (c) SARAL (Ka-band) 0743 (red) track and Jason-2 (Ku and C-bands) 007 (dark green and black) and 120 (light green and gray) tracks between February 2013 and August 2014 and, (d) ENVISAT (Ku and S bands) 0386 (dark green and dark blue) and 0743 (light green and light blue) tracks between June 2002 and October 2010 over Saharian stone desert. (For interpretation of the references to color in this figure legend, the reader is referred to the web version of this article.)

Table 3
Mean and standard deviation (Std) of the backscattering coefficients from Jason-2 (Ku and C bands), between February 2013 and August 2014 over the West African study sites showing temporal stable radar responses.

Sites	Track	Jason-2 (Ku)		Jason-2 (C)	
		Mean (dB)	Std (dB)	Mean (dB)	Std (dB)
Saharian Stone desert	007	19.25	0.53	26.81	0.28
	120	19.06	0.40	26.19	0.40
Saharian Sand desert	172	14.54	0.65	20.54	0.41
	211	17.15	0.49	22.33	0.27
Non flooded tropical evergreen forest	020	3.77	0.80	6.96	0.84

from ~21 dB to ~4.5 dB. The difference in backscattering is ~5.5 dB between C and Ku bands using Jason-2 data and ~4.5 dB between S and Ku bands using ENVISAT data (Tables 2 and 3). The value of difference obtained using Jason-2 is lower than the one obtained using Topex/Poseidon (T/P) data (~9 dB in Papa et al., 2003) when comparing C and Ku bands. This difference can be attributed to the difference in the altimeter waveforms processing (Ice-1 algorithm for Jason-2 in this study, Ocean algorithm for T/P in Papa et al., 2003). More variability is also observed in the radar altimetry backscattering signal when there is an increasing in frequency at each orbit altitude, especially in Ka-band (Tables 2 and 3), that can be attributed to changes in wind intensity and directions that modify roughness of the sand dunes.

4.1.3. Savannahs

Time series of σ_0 over savannahs exhibit a well-marked seasonal signal characterized by an increase of backscattering during the wet season (Figs. 4–7). The length and the intensity of the wet season increase from north (Saharo–Sahelian savannah) to south (Soudanian savannah). Time variations of σ_0 seem related to soil moisture changes as already observed at C and Ku bands using Jason-2 and ENVISAT data over West Africa (Fatras et al., 2012, 2015). The average value of σ_0 during the dry season generally decreases with the frequency, whereas the amplitude of the variations between the wet and dry seasons increases with the frequency, and soil moisture (Figs. 4–7). Changes in amplitude between dry and wet season can reach up to 30 dB after a large rain event (Fig. 6). These time variations over semi-arid areas were related to SSM changes (Cudlip et al., 1994; Ridley et al., 1996; Papa et al., 2003). ENVISAT RA-2 backscattering coefficients were also even recently used to retrieve SSM in semi-arid environment using a linear relationship between the two quantities (Bramer and Berry, 2010; Fatras et al., 2012). We computed linear correlations between σ_0 at the different frequency bands and SSM from AMSR-E between 2003 and 2010 and SMOS between 2013 and 2014. Due to the limited number of data available for SARAL (15 cycles), we computed the linear correlations with SSM up to 3 days after the altimetry pass over each savannah site to have a sufficient number of data. The results are presented in Table 4 for SARAL and ENVISAT and 5 for Jason-2. Due to the important evaporation rates over semi-arid areas, and the very scarce rainfall over the Saharo–Sahelian region, we do not present the results over these sites as they have no significance. When the results are significant (p-value < 0.05), σ_0 are highly correlated to SSM at Ka-band ($R \geqslant 0.65$) in spite of the very short time period of the available records. For the bi-frequency missions (ENVISAT and Jason-2), correlations are higher at the lower frequency (S and C respectively).

4.1.4. Non-flooded tropical evergreen forest

Radar altimetry backscattering coefficients present a quite stable behavior over non flooded tropical evergreen forest (Fig. 8). Their average values decrease from ~17 dB at Ka-band to ~4 dB at Ku-band using Jason-2 data. The difference in backscattering is ~3 dB between C and Ku bands using Jason-2 data and ~0.5 dB between S and Ku bands using ENVISAT data (Tables 2 and 3). A large variability of σ_0 is observed using ENVISAT data from June 2002 to March 2007 (cycles 6–56). Then the variability of σ_0 is very similar to that of Jason-2. A larger variability is also observed at Ka-band (std = 2.94 dB compared to std = 0.80 dB at Ku-band using Jason-2 data, see Table 2), with a time series presenting higher values in April and from November to January, during the wet seasons of the Congo Basin.

4.1.5. Temporarily flooded tropical evergreen forest

Time series of σ_0 in temporarily flooded tropical evergreen forest present a well-marked bimodal signal presenting a maximum

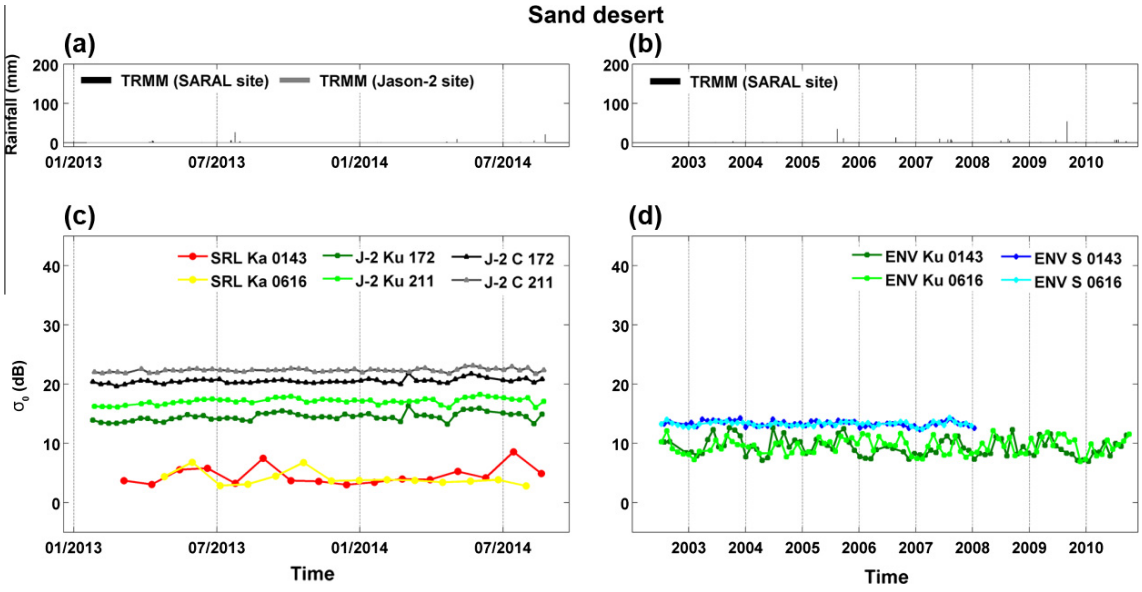

Fig. 3. Time series of daily rainfall (mm) from TRMM 3B423 v7 at (a) SARAL (black) and Jason-2 (gray) sites, (b) ENVISAT site (black). Time series of backscattering coefficient (dB) for (c) SARAL (Ka-band) 0143 (red) and 0616 (yellow) tracks and Jason-2 (Ku and C-bands) 172 (dark green and black) and 211 (light green and gray) tracks between February 2013 and August 2014 and, (d) ENVISAT (Ku and S bands) 0143 (dark green and dark blue) and 0616 (light green and light blue) tracks between June 2002 and October 2010 over Saharian sand desert. (For interpretation of the references to color in this figure legend, the reader is referred to the web version of this article.)

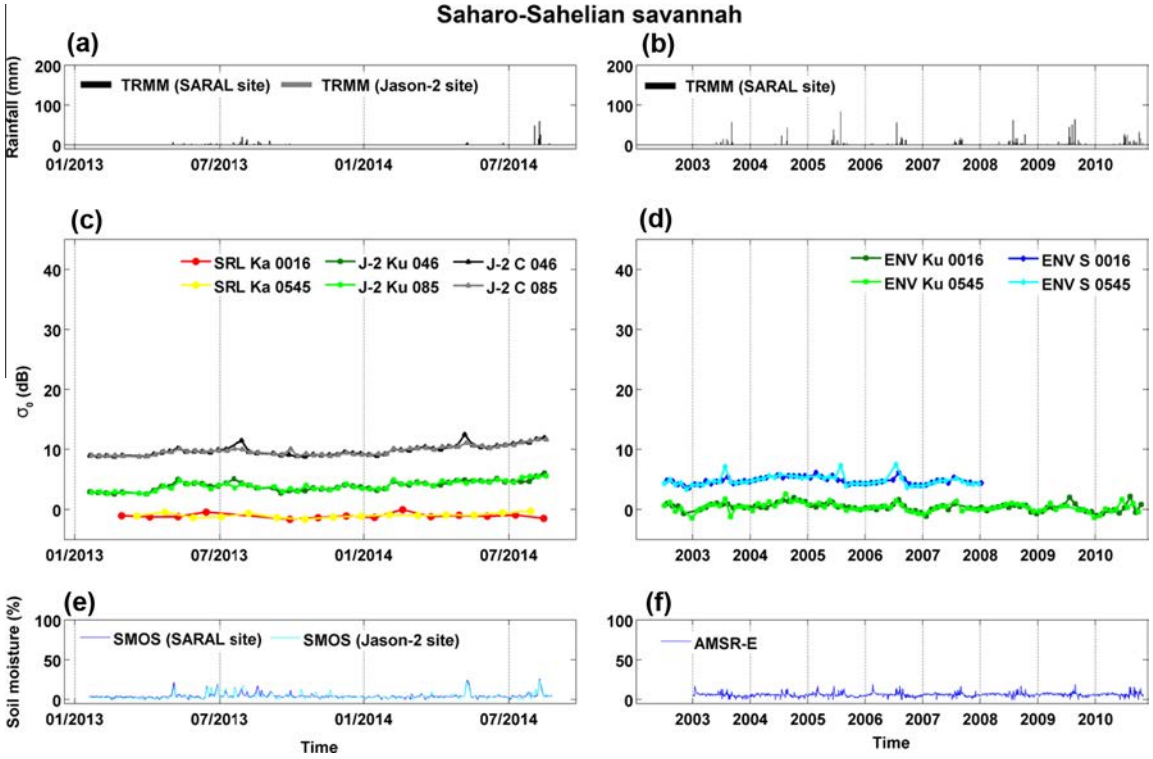

Fig. 4. Time series of daily rainfall (mm) from TRMM 3B423 v7 at (a) SARAL (black) and Jason-2 (gray) sites, (b) ENVISAT site (black). Time-series of backscattering coefficient (dB) for (c) SARAL (Ka-band) 0016 (red) and 0545 (yellow) tracks and Jason-2 (Ku and C-bands) 046 (dark green and black) and 085 (light green and gray) tracks between February 2013 and August 2014 and, (d) ENVISAT (Ku and S bands) 0016 (dark green and dark blue) and 0545 (light green and light blue) tracks between June 2002 and October 2010 over Saharo–Sahelian savannah. Time series of volumetric soil moisture (%) (e) from SMOS at SARAL (blue) and Jason-2 (light blue) sites and (f) from AMSR-E (blue). (For interpretation of the references to color in this figure legend, the reader is referred to the web version of this article.)

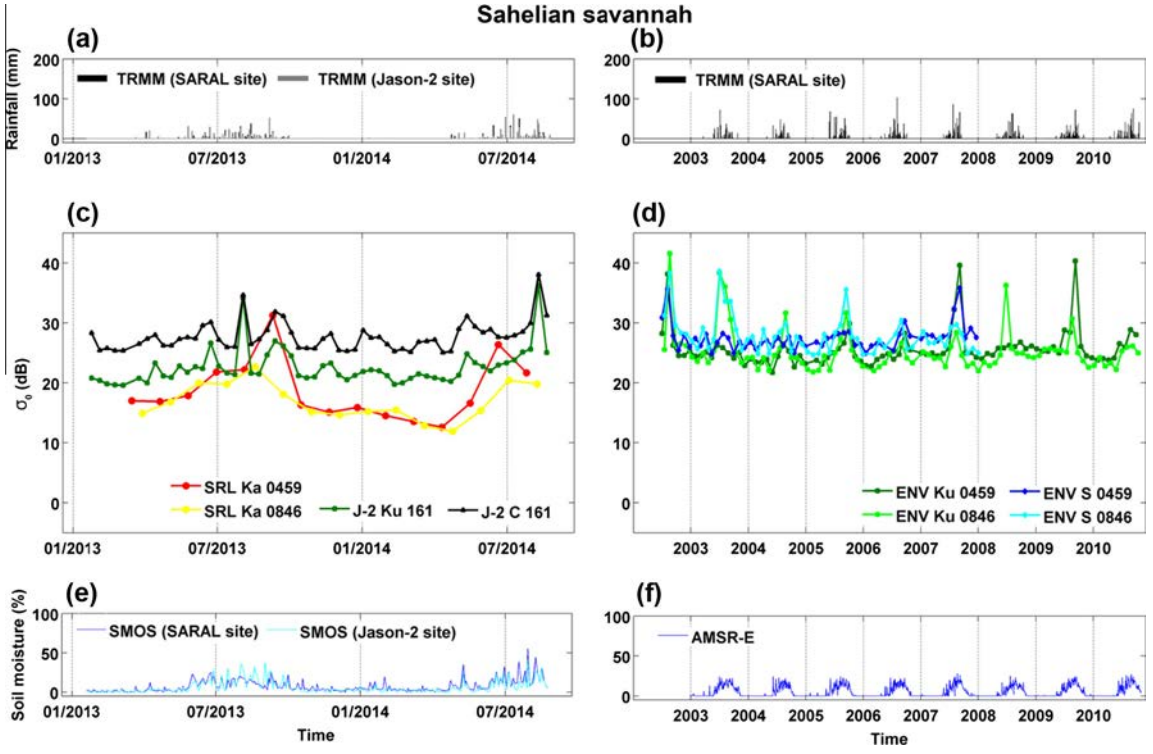

Fig. 5. Time series of daily rainfall (mm) from TRMM 3B423 v7 at (a) SARAL (black) and Jason-2 (gray) sites, (b) ENVISAT site (black). Time-series of backscattering coefficient (dB) for (c) SARAL (Ka-band) 0459 (red) and 0846 (yellow) tracks and Jason-2 (Ku and C-bands) 161 (black and dark green) tracks between February 2013 and August 2014 and, (d) ENVISAT (Ku and S bands) 0459 (dark green and dark blue) and 0846 (light green and light blue) tracks between June 2002 and October 2010 over Sahelian savannah. Time series of volumetric soil moisture (%) (e) from SMOS at SARAL (blue) and Jason-2 (light blue) sites and (f) from AMSR-E (blue). (For interpretation of the references to color in this figure legend, the reader is referred to the web version of this article.)

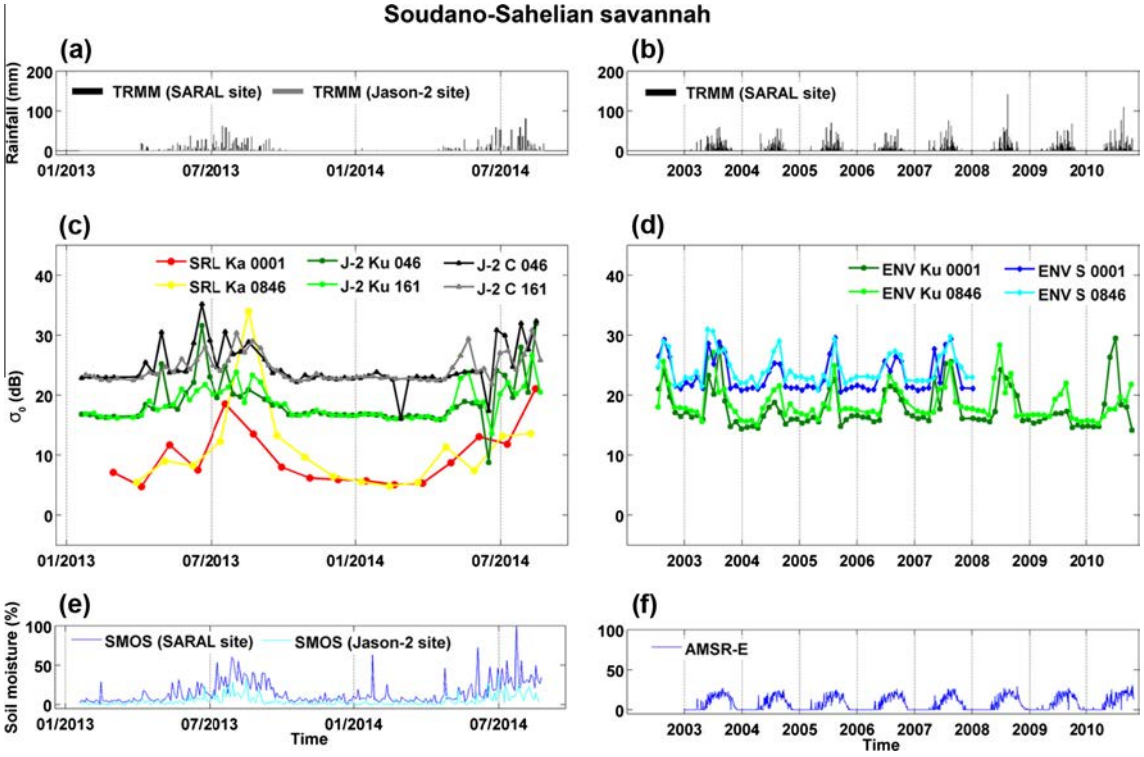

Fig. 6. Time series of daily rainfall (mm) from TRMM 3B423 v7 at (a) SARAL (black) and Jason-2 (gray) sites, (b) ENVISAT site (black). Time-series of backscattering coefficient (dB) for (c) SARAL (Ka-band) 0001 (red) and 0846 (yellow) tracks and Jason-2 (Ku and C-bands) 046 (dark green and black) and 161 (light green and gray) tracks between February 2013 and August 2014 and, (d) ENVISAT (Ku and S bands) 0001 (dark green and dark blue) and 0846 (light green and light blue) tracks between June 2002 and October 2010 over Soudano-Sahelian savannah. Time series of volumetric soil moisture (%) (e) from SMOS at SARAL (blue) and Jason-2 (light blue) sites and (f) from AMSR-E (blue). (For interpretation of the references to color in this figure legend, the reader is referred to the web version of this article.)

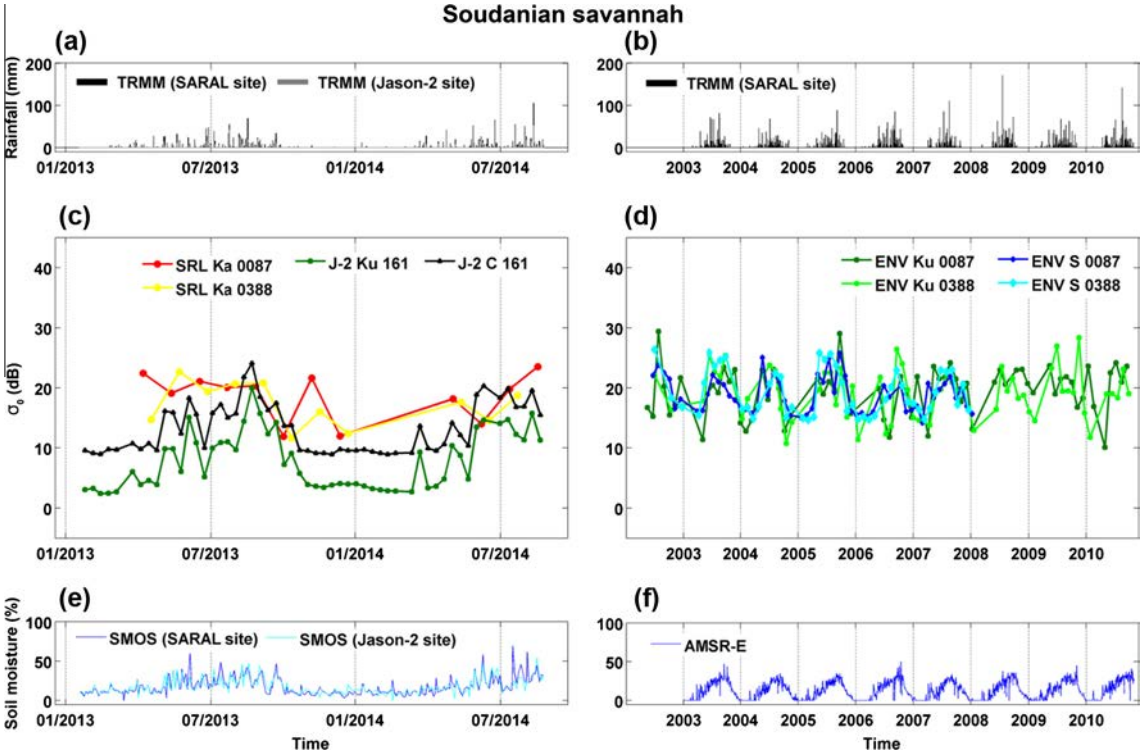

Fig. 7. Time series of daily rainfall (mm) from TRMM 3B423 v7 at (a) SARAL (black) and Jason-2 (gray) sites, (b) ENVISAT site (black). Time-series of backscattering coefficient (dB) for (c) SARAL (Ka-band) 0087 (yellow) and 0388 (red) tracks and Jason-2 (Ku and C-bands) 161 (dark green and black) tracks between February 2013 and August 2014 and, (d) ENVISAT (Ku and S bands) 0087 (dark green and dark blue) and 0388 (light green and light blue) tracks between June 2002 and October 2010 over Soudanian savannah. Time series of volumetric soil moisture (%) (e) from SMOS at SARAL (blue) and Jason-2 (light blue) sites and (f) from AMSR-E (blue). (For interpretation of the references to color in this figure legend, the reader is referred to the web version of this article.)

Table 4
Correlation coefficients (R) and significance threshold at 95% (p) between radar altimetry backscattering coefficients and Surface Soil Moisture (SSM) over the savannah sites. The number of observations is also indicated (Nb).

Savannah sites	Track	SARAL (Ka)		ENVISAT (Ku)		ENVISAT (S)	
		R (p)	Nb	R (p)	Nb	R (p)	Nb
Sahelian	0459	0.64 (0.018)	13	0.64 (<0.001)	74	0.66 (<0.001)	45
	0846	0.68 (0.008)	14	0.60 (<0.001)	77	0.60 (<0.001)	48
Soudano-Sahelian	0001	0.88 (<0.001)	15	0.50 (<0.001)	75	0.71 (<0.001)	46
	0846	0.53 (0.05)	14	0.62 (<0.001)	77	0.75 (<0.001)	48
Soudanian	0087	0.35 (0.263)	12	0.38 (<0.001)	54	0.67 (<0.001)	42
	0388	0.84 (0.04)	9	0.47 (<0.001)	56	0.72 (<0.001)	43

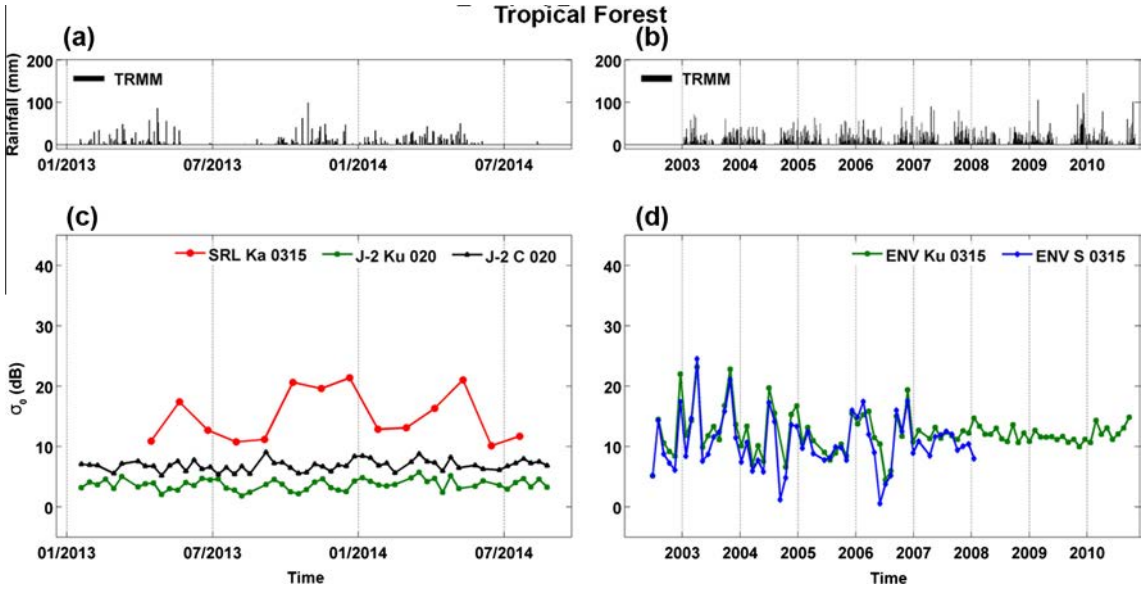

Fig. 8. Time series of daily rainfall (mm) from TRMM 3B423 v7 at (a) SARAL (black) and Jason-2 (gray) sites, (b) ENVISAT site (black). Time-series of backscattering coefficient (dB) for (c) SARAL (Ka-band) 0315 (red) tracks and Jason-2 (Ku and C-bands) 020 (dark green and black) track between February 2013 and August 2014 and, (d) ENVISAT 0315 (Ku – dark blue – and S – dark green-bands) track between June 2002 and October 2010 over non flooded evergreen tropical forest. (For interpretation of the references to color in this figure legend, the reader is referred to the web version of this article.)

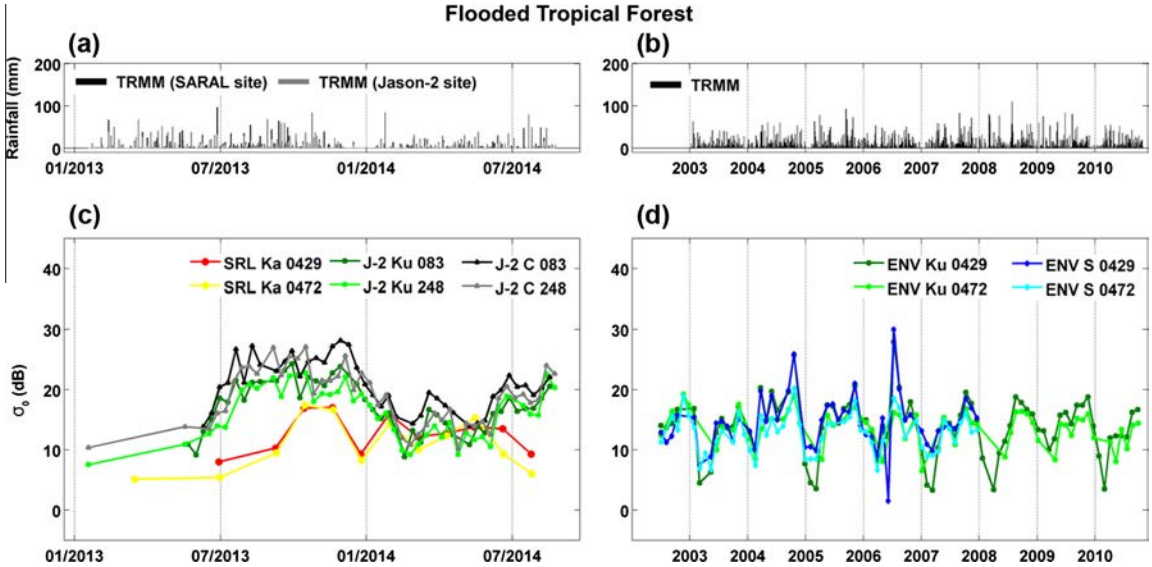

Fig. 9. Time series of daily rainfall (mm) from TRMM 3B423 v7 at (a) SARAL (black) and Jason-2 (gray) sites, (b) ENVISAT site (black). Time-series of backscattering coefficient (dB) for (c) SARAL (Ka-band) 0429 (red) and 0472 (yellow) tracks and Jason-2 (Ku and C-bands) 083 (dark green and black) and 248 (light green and gray) tracks between February 2013 and August 2014 and, (d) ENVISAT (Ku and S bands) 0429 (dark green and dark blue) and 0472 (light green and light blue) tracks between June 2002 and October 2010 over temporarily flooded evergreen tropical forest. (For interpretation of the references to color in this figure legend, the reader is referred to the web version of this article.)

occurring in November–December, a secondary maximum in April–May, and minimums in February–March, and between June and August depending on the locations of the study sites (Fig. 9). The time variations are well correlated to the hydrological regime of the Congo River and its tributaries in the Cuvette Centrale and associated flooding patterns (e.g., Betbeder et al., 2014). Minimums recorded in summer occur earlier (June) in the Jason-2 subsite than in the ENVISAT/SARAL one (August) due to its location in the upstream part of the basin. The amplitude of the variations during the floods is around 10 dB for each frequency band, and the minimums of backscattering are similar to the ones observed for non flooded tropical evergreen forest.

4.2. Spatio-temporal variations of backscattering along the meridian transects

The latitudinal variations of the backscattering coefficient over the Niger inner delta between 13° and 17°N are represented as a function of time at Ka-band for SARAL track 0474 (Fig. 10a) and at C- and Ku-bands for Jason-2 track 046 between February 2013 and January 2014 time-period (Fig. 11a and b) and at Ku- and S-bands for ENVISAT track 0474, between June 2002 and October 2010 at Ku-band (Fig. 10b) and between June 2002 and January 2008 at S-band (Fig. 10c). The locations of the altimeter tracks are shown in Fig. 1b.

SARAL/ENVISAT track 0474 crosses, from north to south, the dried since 2000 Lake Faguibine, in northern Mali, between 16.75°N and 16.65°N, and the inundated areas of the Niger inner delta from 15.85°N to 13.10°N. Large variations of backscattering can be observed between the low (October – January) and high (February – September) water periods at Ka (Fig. 10a), Ku (Fig. 10b), and S (Fig. 10c) bands, especially in the central part of the delta between 13.75°N and 15.5°N, where the backscattering can reach up to 50 dB during the flood peak. The difference of backscattering between Ku and S bands reveals important latitudinal and seasonal variabilities. Differences of 7–15 dB are observed in the north, between 16.5°N and 17°N, larger during the wet than during the dry season. These values correspond to what was observed over Sahelian and Saharo–Sahelian savannahs (Figs. 4 and 5). In the central part of the delta, close to 0 and slightly negative values are observed during the low water period whereas positive values are obtained during high water period. The larger the flood is, the higher the difference of backscattering is.

The spatio-temporal variations at Ku and C bands along Jason-2 track 046 are very similar to the ones at Ku and S bands for ENVISAT track 0474 for the northern part of the transect between 15.5°N and 17°N as the two tracks cross similar landscapes (Fig. 11). Very high σ_0 (>50 dB) values are present between 16.15°N and 16.25°N, corresponding to the Oro Lake. Below 15.5°N, the Jason-2 track crosses landscapes composed of savannahs and sandy dunes. Their σ_0 variations are typical of these types of surface (see Figs. 3–5 and Fatras et al., 2015). High values of σ_0 are also observed during the wet season (July to September), likely due to a rain event occurring just before the satellite overflight.

4.3. Time-variations of water levels and backscattering

Changes in σ_0 values were compared to temporal variations of the water levels for two locations in the Inner Niger Delta. Time series of altimetry-based water levels were obtained at the intersections of ENVISAT/SARAL track 0932 and Jason-2 track 046 and the Niger River using MAPS (Frappart et al., in press). Altimetry-based water levels were first validated against records from the Diré (located 10.3 km downstream intersections of ENVISAT/SARAL track 0932 and the Niger River) and the Tonka (located 10.2 km downstream intersections of Jason-2 track 046

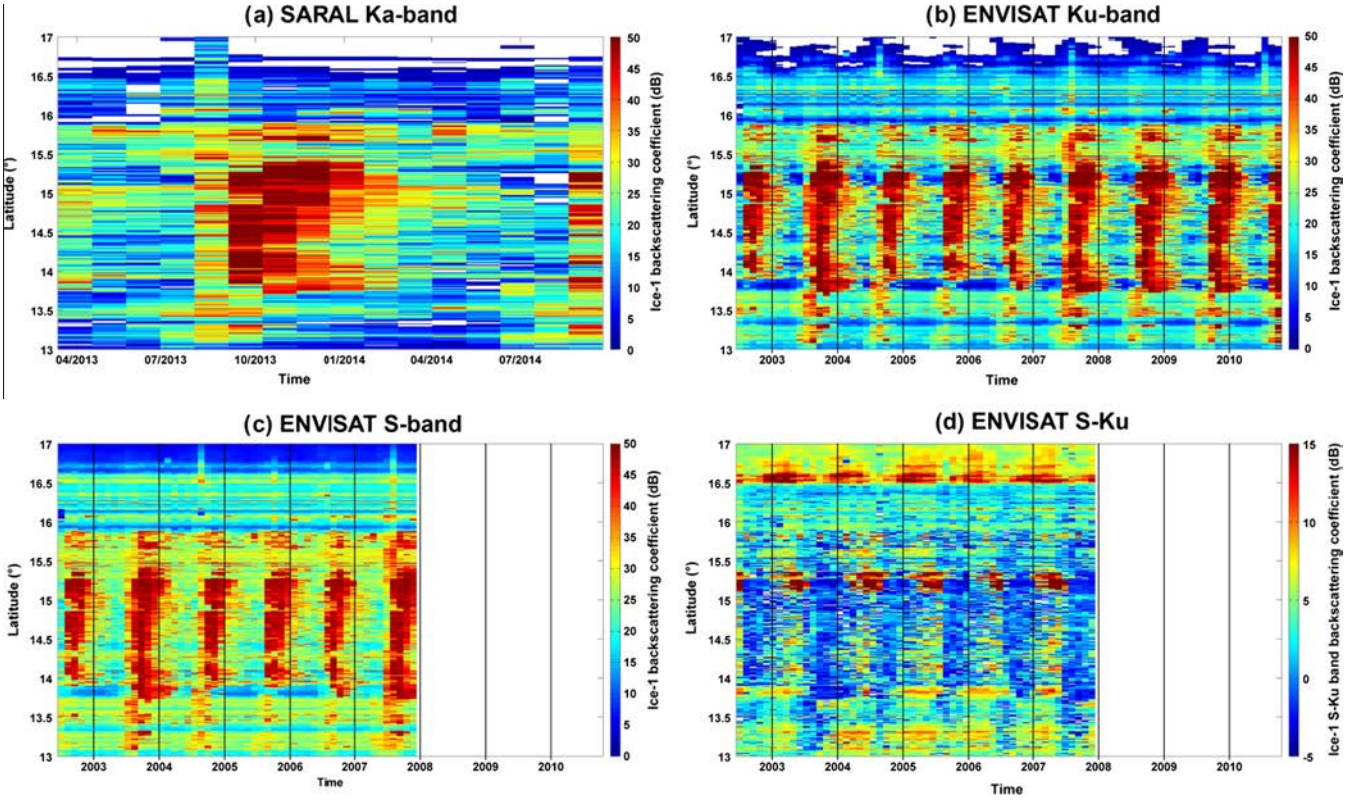

Fig. 10. Time–space diagrams illustrating the variations of backscattering coefficients (dB) from track 0474 at (a) Ka-band from SARAL between February 2013 and August 2014, (b) Ku-band between June 2002 and October 2010, (c) S-band and (d) S-Ku-S from ENVISAT between June 2002 and January 2008.

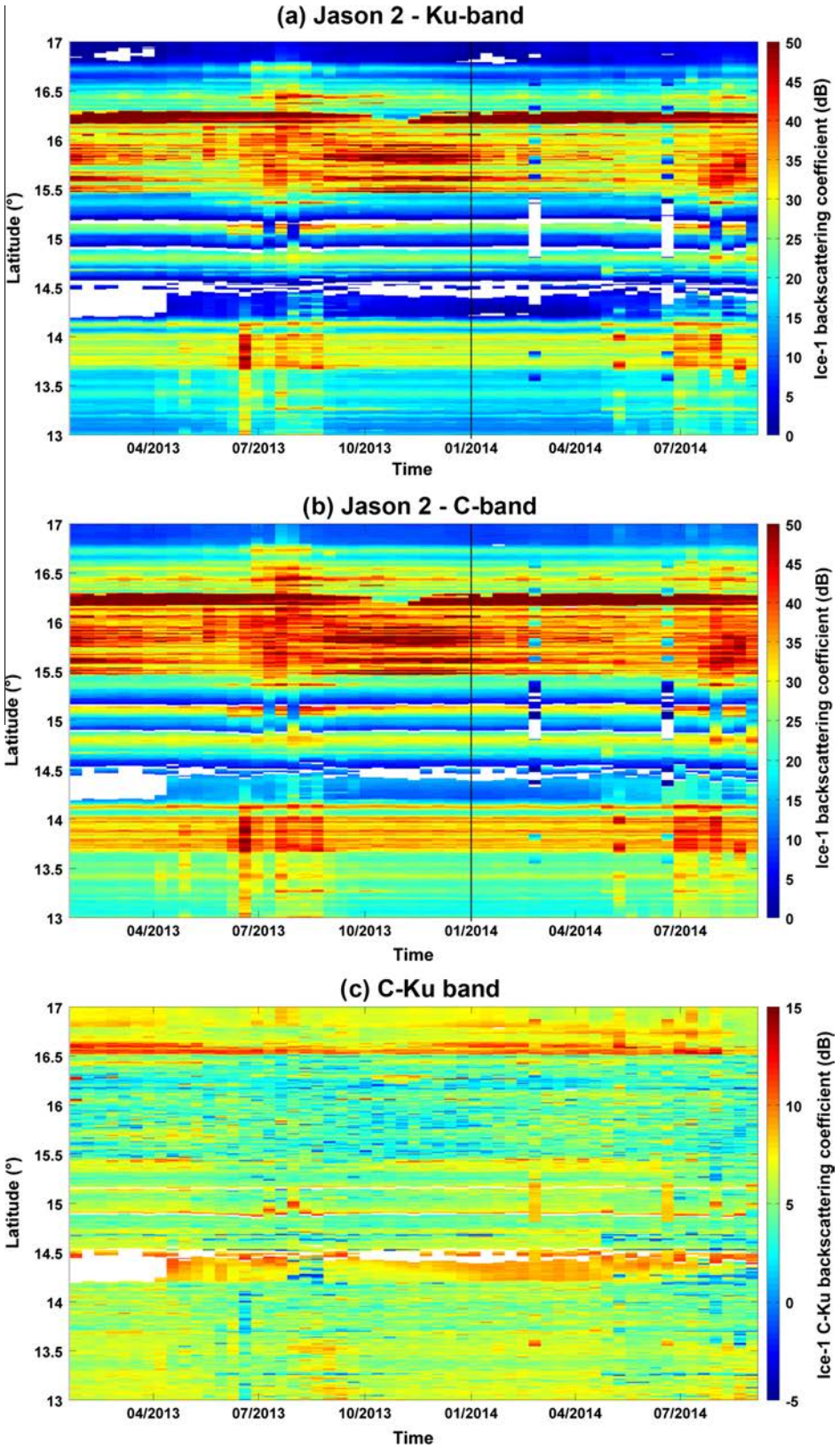

Fig. 11. Time–space diagrams illustrating the variations of backscattering coefficients (dB) from Jason-2 track 046 at (a) Ku-band, (b) C-band between and (c) C-Ku between February 2013 and August 2014.

and the Niger River) *in situ* gauge stations over their common period of availability (i.e., January 2009–October 2010 for ENVISAT, January 2013–August 2014 for SARAL and January 2009–December 2010 for Jason-2). ENVISAT/SARAL track 0932 crosses the Niger River along 700 m and Jason-2 track 046 crosses the Niger River along 1.5 km. Altimetry-based time series of water

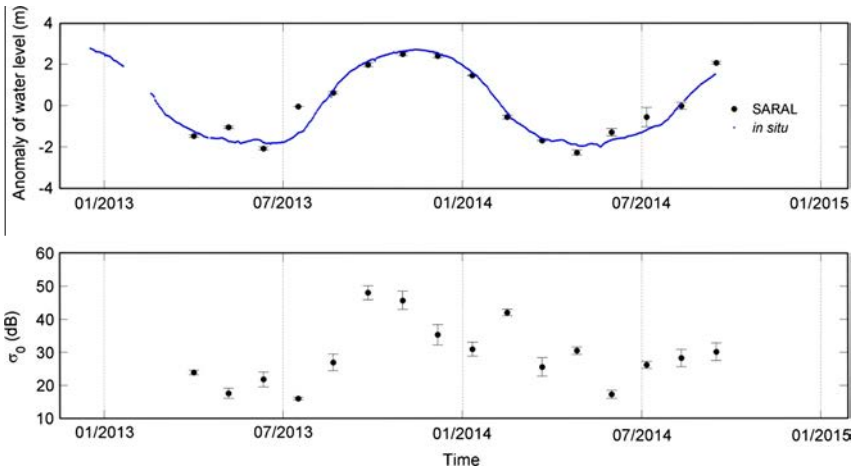

Fig. 12. (a) Time series of water levels based on SARAL data from track 0932 (black circles) and from Diré gauge records (blue dots). (b) Time series of backscattering measurements at Ka-band from SARAL. (For interpretation of the references to color in this figure legend, the reader is referred to the web version of this article.)

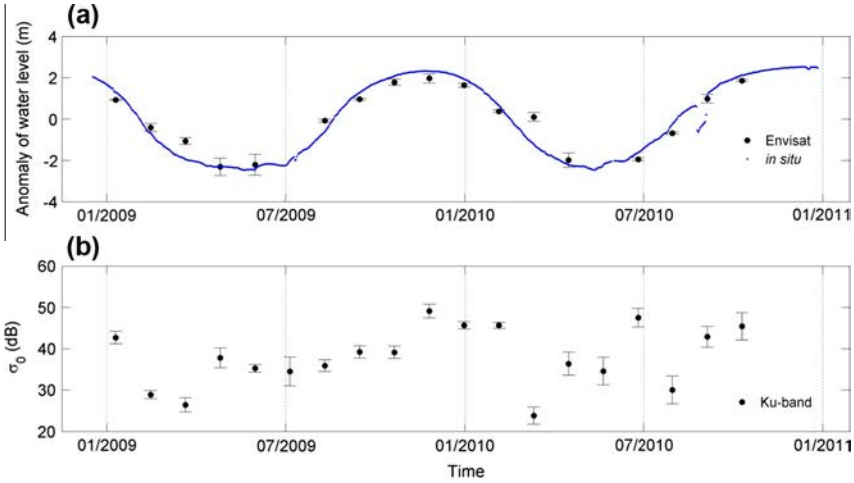

Fig. 13. (a) Time series of water levels based on ENVISAT data from track 0932 (black circles) and from Diré gauge records (blue dots). (b) Time series of backscattering measurements at Ku-band from ENVISAT. (For interpretation of the references to color in this figure legend, the reader is referred to the web version of this article.)

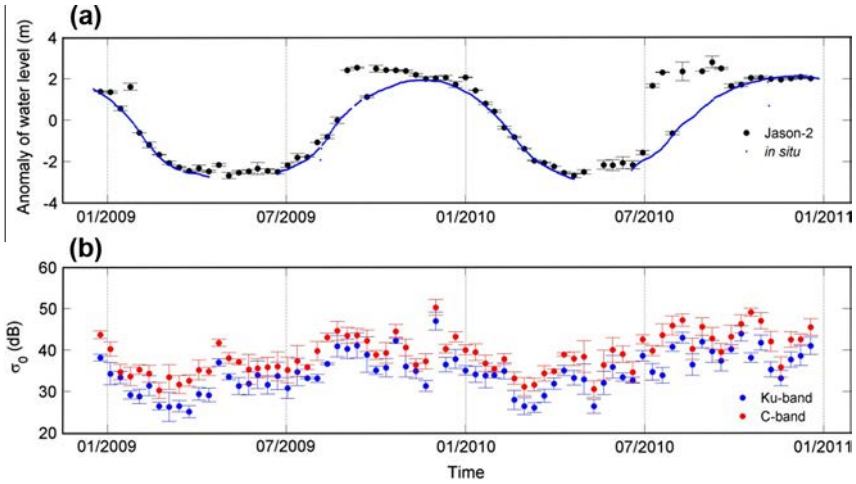

Fig. 14. (a) Time series of water levels based on Jason-2 data from track 046 (black circles) and from Tonka gauge records (blue dots). (b) Time series of backscattering measurements at Ku (blue) and S C (red) bands from Jason-2. (For interpretation of the references to color in this figure legend, the reader is referred to the web version of this article.)

levels exhibit very similar variations to *in situ* gauges records (Figs. 12a, 13a, and 14a). Comparisons between both sources present correlations of 0.97, 0.96, 0.90, and RMSE of 0.47, 0.50, 0.82 m using SARAL, ENVISAT, Jason-2 data. Performances of Jason-2 for retrieving water levels are quite lower because the virtual station is located on the Niger mainstem whereas the Tonka tide gauge is located on the tributary flowing from the Oro Lake to the Niger, close to the junction with the Niger River. As a consequence, the high water period is shorter on this tributary than in the mainstem. This explains the lower correlation value and the higher RMSE obtained using Jason-2 data. The time series of backscattering coefficients from SARAL at Ka-band, ENVISAT at Ku-band (S-band data are not valid after January 2008), and Jason-2 at Ku and C bands are presented in Figs. 12b, 13b, and 14b respectively. They exhibit similar patterns of temporal variations as water levels, with higher σ_0 values reaching 45 –50 dB during the high water season (Figs. 12b, 13b, and 14b). During the low water season, σ_0 values can decrease to ~25 dB at Ka and Ku bands and ~30 dB at C-band.

5. Discussion

Backscattering coefficients acquired at Ka, Ku, C and S bands present a wide range of spatio-temporal variations over West Africa. They can be related to the spatio-temporal changes in roughness and dielectric constant of the upper soil surface. σ_0 values decrease as the frequency increases (or the wavelength decreases), except over non-flooded evergreen tropical forest at Ka-band. Previous studies demonstrated the capability of Ka-band nadir-looking radars for the detection of targets below the canopy (Nashashibi et al., 2004). It is due to the predominance of soil over vegetation returns for nadir and low incidence angles at Ka-band, especially for a wet soil as in tropical humid forest (Waite and MacDonald, 1971). The amplitude of the variations in backscattering between the dry and the wet seasons increases with the frequency, as previously observed by Fatras et al. (2012, 2015). This is contradictory with experiments showing that the real part of the dielectric constant that is directly related to the reflectivity of the ground decreases with frequency for a given wetness (Hallikainen et al., 1985). This opposite behavior of the Ka-band results from the size of the altimeter footprint that increases as frequency decreases for a given altitude. As the size of the footprint increases, it becomes less and less homogeneous encompassing a mix of surfaces with different SSM, reducing the maximum amplitude of the annual backscattering.

A part of the variability observed in the ENVISAT and SARAL time series is related to the orbit of the satellites. Improvements in the orbit control of ENVISAT satellite permitted to reduce the deviation to the nominal track from 1 km to less than 250 m since April 2007 (Kuijper and Garcia Matatoros, 2007) that account for the reduction of the variability over the different study sites (see its impact of the non flooded evergreen forest in Fig. 8). SARAL did not precisely follow the ENVISAT orbit during its four first cycles (February to July 2013). Deviations of several kilometers from the nominal orbit were found. This is likely to account for a part of the variability observed in northern hemisphere spring and the beginning of summer 2013 over all the sites.

Biases can be observed in the radar echoes in the same frequency band between the ascending and the descending tracks for the same study site (Figs. 2–9). Apart from the differences that can be caused by the time sampling, they are caused by the fact that the surface observed for each track is different as the diameter of the altimeter footprint varies from a few (Ka-band) to several tenths of kilometers (Ku, C and S bands).

Over deserts, the stability of the backscattering response decreases as frequency increases (Figs. 2 and 3 and Tables 2 and 3). These variations are due to changes in surface pattern and roughness caused by the winds according to results from electromagnetic modeling studies (Stephen and Long, 2005, 2007) and were also previously observed over the same sites using radar scatterometry data (Fatras et al., 2015). This effect is smaller over stone deserts that are covered with a thin layer of sand than other sand deserts. If these changes in roughness do not affect radar altimetry backscattering signatures at lower frequency (i.e., higher wavelength) in S, C, and Ku bands, they have a higher impact at Ka-band for wavelength lower than one cm. The differences between C- and Ku-bands using Jason-2 data and between S- and Ku-bands using ENVISAT data are typical of sand desert and can be related to the difference of penetration depths at C- and Ku-bands and S- and Ku-bands over sand dunes and arid regions (Ulaby et al., 1982, 1986), along with different antenna apertures and footprints, the latter depending on the wavelength and the antenna diameter. The differences in antenna apertures and footprints between ENVISAT and Jason-2, along with the different locations of the two sub-sites are responsible for the differences in backscattering at Ku-band between the two altimeters. The small differences between both tracks may be accounted for the different sand dunes pattern below the two satellite path over the integration area, and their variation over time (Stephen and Long, 2005).

Over savannahs, the backscattering coefficients from SARAL are generally well correlated to SSM obtained using passive microwave measurements from SMOS (Table 4). Measurements from one of the track appear less correlated to SSM than the measurements from the other. Two main reasons account for these discrepancies: the changes in the orbit during the four first cycles, the difference in spatial scales and between the two sources of information, and the methodology used for comparisons. Given the large spatio-temporal variability of SSM in semi-arid environments, changes in the scene observed by the satellite cause differences in the radar response, for example when a localized rain event is detected in one source and not in the other, especially when the comparison is performed on a 3-day time-window. Diminishing the length of the time-window permits to increase the R value up to 0.98 at the expense of reducing the number of comparisons down to 6.

Radar waves are less affected by the vegetation cover at lower frequencies (C and S for Jason-2 and ENVISAT respectively) than at higher frequency (Ku) even in nadir-looking configuration (Tables 4 and 5). Nevertheless, the highest correlations were obtained at Ka-band for Soudano-Sahelian ($R = 0.88$ for SARAL track 0001) and Soudanian ($R = 0.84$ for SARAL track 0388) savannah sites. This is in good agreement with previous studies showing the capability of nadir-looking radars for detecting surface responses below vegetation (Waite and MacDonald, 1971; Nashashibi et al., 2004).

Over Sahelian savannahs, similar results are obtained when comparing Ku- and S-bands to SSM, whereas a much better

Table 5
Correlation coefficients (R) and significance threshold at 95% (p) between radar altimetry backscattering coefficients and Surface Soil Moisture (SSM) over the savannah sites. The number of observations is also indicated (Nb).

Savannah sites	Track	Jason-2 (Ku)		Jason-2 (C)	
		R (p)	Nb	R (p)	Nb
Sahelian	161	0.76 (<0.001)	54	0.69 (<0.001)	54
Soudano-Sahelian	046	0.48 (<0.001)	51	0.58 (<0.001)	52
	161	0.43 (0.002)	52	0.47 (<0.001)	52
Soudanian	161	0.67 (<0.001)	52	0.68 (<0.001)	52

agreement was found between σ_0 at Ku-band and *in-situ* measurements than at S-band (Fatras et al., 2012). Due to the difference in footprint size at Ku- and S-bands, σ_0 at Ku-band are more correlated to local measurements whereas σ_0 at S-band are more correlated to regional estimates of SSM.

Radar responses at Ku-, C- and S-bands are stable over non flooded tropical forests. If the EM wave can penetrate the dense canopy cover, the backscattered power is not sufficient to go through the canopy a second time (Fig. 8). Signals received by the altimeter are the ones scattered on the canopy surface at Ku-band or affected by multiple scattering in the vegetation caused by the leaves, branches and trunks and by also volume scattering at C- and S-bands (Ulaby et al., 1986). The almost constant $\sigma_0 \sim 7$ dB observed in the Jason-2 time series corresponds to the saturation level at C-band due to volume scattering (e.g., Frison and Mougin, 1996a,b). At higher frequency as in Ka-band, the attenuation of the electro-magnetic waves by the foliage is larger. But at nadir incidence, previous studies showed that millimeter electromagnetic waves were able to penetrate underneath foliage-cover, even for dense canopy cover (Waite and MacDonald, 1971; Nashashibi et al., 2004). As a consequence, higher σ_0 response is observed during the wet season over non-flooded (Fig. 8) tropical evergreen forests as the dielectric constant and so the ground reflectivity is increasing with the water content (Hallikainen et al., 1985). Similarly, the presence of water below the canopy during the flood in temporarily flooded tropical evergreen forests causes a huge change of the ground reflectivity. An increase of the σ_0 in all the bands during the flood season (Fig. 9) showing the capability of radar altimetry to detect water under the canopy, and accounting for the monitoring of water levels in forested wetlands temporarily or permanently inundated reported in previous studies (e.g., Frappart et al., 2008, 2011; Santos da Silva et al., 2010, 2012).

In the Inner Niger Delta, temporal variations of the backscattering coefficients are related to the flood regime over temporarily inundated areas and to SSM over non-inundated areas (Figs. 10 and 11). Variations in σ_0 greater than 25 dB were found between high and low water periods in the inundated areas (Figs. 10 and 11) and over the Niger River (Figs. 12b, 13b, and 14b). Considering the differences between frequency (C and Ku with Jason-2 and S and Ku with ENVISAT), it also appears that bare and dry soils exhibit higher backscattering responses (>3 dB) than inundated areas and wet soils and/or covered with vegetation as previously observed (Fatras et al., 2015).

6. Conclusion

Altimetry radar signatures from SARAL (Ka-band), Jason-2 (Ku and C-bands), and ENVISAT (Ku and S-bands) were analyzed over West Africa. The altimeter backscattered responses at Ka-, Ku-, C- and S-bands exhibit a wide range of spatial and temporal variations over this region. Radar altimetry backscattering coefficients vary from 0 dB to 50 dB over the various land surfaces present along the West African bioclimatic gradient. The backscattered energy by each surface can be related to its soil roughness and soil dielectric constant and their variations against time. Over land surfaces with bio-physical properties not varying against time, as stone and sand deserts and non-inundated evergreen tropical forests, radar altimeters exhibit quite stable responses. The higher frequencies (Ku and Ka) are yet more affected by changes in roughness caused by the wind regime over deserts. Besides, Ka-band demonstrates a strong sensitivity to moisture variations underneath the canopy of tropical evergreen forest. Over savannahs, radar altimetry confirms its strong potential for the monitoring of SSM in semi-arid areas already demonstrated by Fatras et al. (2012). Differences in frequency C–Ku and S–Ku are likely to make easier the distinction between wet and dry soils and/or bare soil and vegetation areas. Backscattering coefficients also provide very useful information for detecting inundated areas in the altimeter groundtracks that could be used to identify altimetry echoes corresponding to a lake, a river or a wetland surface.

If the use of radar altimetry for the monitoring of land surfaces currently suffers from its low spatial and temporal resolutions, the launch of the Surface Water and Ocean Topography (SWOT) mission in 2020 will permit to overcome the limitations. Using the SAR interferometry technique at near nadir incidences, SWOT will provide backscattering coefficients in a swath of ~120 km with a spatial resolution of 100 m over land.

Conflict of interest

There is no conflict of interest.

Acknowledgements

C. Fatras is supported by a CNES/ONERA PhD grant. This work was supported by the Programme National de Télédétection Spatiale (PNTS, http://www.insu.cnrs.fr/actions-sur-projets/pnts-programme-national-de-teledetection-spatiale), grant n° PNTS-2012-03. We thank two anonymous Reviewers for their helpful comments that helped us in improving the quality of this study.

References

Baup, F., Mougin, E., de Rosnay, P., Timouk, F., Lavenu, F., Chênerie, I., 2007. Surface soil moisture estimation over the AMMA sahelian site in Mali using ENVISAT/ASAR data. Remote Sens. Environ. 109, 473–481.

Baup, F., Mougin, E., de Rosnay, P., Hiernaux, P., Frappart, F., Frison, P-L., Zribi, M., Viarre, J., 2011. Mapping surface soil moisture over the Gourma mesoscale site (Mali) by using ENVISAT ASAR data. Hydrol. Earth Syst. Sci. 15 (2), 603–616.

Betbeder, J., Gond, V., Frappart, F., Baghdadi, N., Briant, G., Bartholome, E., 2014. Mapping of Central Africa forested wetlands using remote sensing. IEEE J. Sel. Top. Earth Observ. Remote Sens. 7 (2), 531–542.

Birkett, C.M., 1995. The contribution of TOPEX/POSEIDON to the global monitoring of climatically sensitive lakes. J. Geophys. Res. 100 (C12), 25179–25204.

Birkett, C.M., 1998. Contribution of the TOPEX NASA Radar Altimeter to the global monitoring of large rivers and wetlands. Water Resour. Res. 34 (5), 1223–1239.

Bramer, S.M.S., Berry, P.A.M., 2010. Soil surface moisture from EnviSat RA-2: from modelling towards implementation. In: Mertikas, S.P. (Ed.), Gravity, Geoid and Earth Observation, IAG Commission 2: Gravity Field, Chania, Part III, Crete, Greece, 23–27 June 2008, pp. 205–212.

Crétaux, J.-F., Jelinski, W., Calmant, S., Kouraev, A., Vuglinski, V., Bergé-Nguyen, M., Gennero, M.-C., Niño, F., Abarca Del Rio, R., Cazenave, A., Maisongrande, P., 2011. SOLS: a lake database to monitor in the Near Real Time water level and storage variations from remote sensing data. Adv. Space Res. 47 (9), 1497–1507.

Cudlip, W., Ridley, J.K., Strawbridge, F., Harris, A., Rapley, C.G., 1994. Detecting surface roughness and moisture variations in deserts. In: Proc. 2nd ERS-1 Symposium, Hamburg 1993, ESA SP-361, pp. 849–853.

Fatras, C., Frappart, F., Mougin, E., Grippa, M., Hiernaux, P., 2012. Estimating surface soil moisture over Sahel using ENVISAT radar altimetry. Remote Sens. Environ. 123 (8), 496–507.

Fatras, C., Frappart, F., Mougin, E., Frison, P.-L., Faye, G., Borderies, P., Jarlan, L., 2015. Spaceborne altimetry and scatterometry backscattering signatures at C- and Ku-band over West Africa. Remote Sens. Environ. 159, 117–133.

Frappart, F., Seyler, F., Martinez, J.M., León, J.G., Cazenave, A., 2005. Floodplain water storage in the Negro River basin estimated from microwave remote sensing of inundation area and water levels. Remote Sens. Environ. 99 (4), 387–399.

Frappart, F., Calmant, S., Cauhopé, M., Seyler, F., Cazenave, A., 2006a. Preliminary results of ENVISAT RA-2 derived water levels validation over the Amazon basin. Remote Sens. Environ. 100 (2), 252–264.

Frappart, F., Do Minh, K., L'Hermitte, J., Cazenave, A., Ramillien, G., Le Toan, T., Mognard-Campbell, N., 2006b. Water volume change in the lower Mekong basin from satellite altimetry and imagery data. Geophys. J. Int. 167 (2), 570–584.

Frappart, F., Papa, F., Famiglietti, J.S., Prigent, C., Rossow, W.B., Seyler, F., 2008. Interannual variations of river water storage from a multiple satellite approach: a case study for the Rio Negro River basin. J. Geophys. Res. 113, D21104.

Frappart, F., Papa, F., Güntner, A., Werth, S., Santos da Silva, J., Tomasella, J., Seyler, F., Prigent, C., Rossow, W.B., Calmant, S., Bonnet, M.-P., 2011. Satellite-based estimates of groundwater storage variations in large drainage basins with extensive floodplains. Remote Sens. Environ. 115 (6), 1588–1594.

Frappart, F., Papa, F., Santos da Silva, J., Ramillien, G., Prigent, C., Seyler, F., Calmant, S., 2012. Surface freshwater storage and dynamics in the Amazon basin during the 2005 exceptional drought. Environ. Res. Lett. 7 (4), 044010.

Frappart, F., Papa, F., Marieu, V., Malbeteau, Y., Jordy, F., Calmant, S., Durand, F., Bala, S., in press. Preliminary assessment of SARAL/AliKa observations over the Ganges-Brahmaputra and Irrawaddy Rivers. Mar. Geodesy.

Frison, P.L., Mougin, E., 1996a. Monitoring global vegetation dynamics with ERS-1 wind scatterometer data. Int. J. Remote Sens. 17 (16), 3201–3218.

Frison, P.L., Mougin, E., 1996b. Use of ERS-1 wind scatterometer data over land surfaces. IEEE Trans. Geosci. Remote Sens. 34, 1–11.

Frison, P.L., Mougin, E., Hiernaux, P., 1998. Observations and interpretation of seasonal ERS-1 wind scatterometer data over northern Sahel (Mali). Remote Sens. Environ. 693, 233–242.

Goita, K., Diepkile, A.T., 2012. Radar altimetry of water level variability in the Inner Delta of Niger River. In: IEEE Int. Geosci. Remote Sens. Symposium 2012 (IGARSS 2012), pp. 5262–5265.

Hallikainen, M.T., Ulaby, F.T., Dobson, M.C., El-Rayes, M.A., Wu, L.K., 1985. Microwave dielectric behavior of wet soil-part 1: empirical models and experimental observations. IEEE Trans. Geosci. Remote Sens. GE-23 (1), 25–34.

Hardin, P.J., Long, D.G., Remund, Q.P., 1996. Discrimination of Africa's vegetation using reconstructed ERS-1 imagery. In: IEEE Int. Geosci. Remote Sens. Symposium 1996. IGARSS'96(2), pp. 827–829.

Huffman, G.J., Adler, R.F., Bolvin, D.T., Gu, G.J., Nelkin, E.J., Bowman, K.P., Hong, Y., Stocker, E.F., Wolff, D.B., 2007. The TRMM multisatellite precipitation analysis (TMPA): quasi-global, multiyear, combined-sensor precipitation estimates at fine scales. J. Hydrometeorol. 8 (1), 38–55.

Huffman, G.J., Adler, R.F., Bolvin, D.T., Nelkin, E.J., 2010. The TRMM Multi-satellite Precipitation Analysis (TMPA). In: Hossain, F., Gebremichael, M. (Eds.), Satellite Rainfall Applications for Surface Hydrology. Springer Verlag, pp. 3–22, ISBN: 978-90-481-2914-0 (Chapter 1).

Isnard, H., 1968. Esquisse du climat de la Libye. Méditerranée 3, 247–260.

Jones, K., Lanthier, Y., Van der Voet, P., Van Valkengoed, E., Taylor, D., Fernandez-Prieto, D., 2009. Monitoring and assessment of wetlands using Earth Observation: the GlobWetland project. J. Environ. Manage. 90 (7), 2154–2169.

Kerr, Y.H., Waldteufel, P., Richaume, P., Wigneron, J.P., Ferrazzoli, P., Mahmoodi, A., et al., 2012. The SMOS soil moisture retrieval algorithm. IEEE Trans. Geosci. Remote Sens. 50, 1384–1403.

Kuijper, D., Garcia Matatoros M.A., 2007. Analysis of Envisat orbit maintenance strategies to improve/increase Envisat ASAR interferometry opportunities. In: 20th International Symposium on Space Flight Dynamics Proc., Annapolis, Maryland, USA, 24–28 September, 2007.

Le Barbé, L., Lebel, T., Tapsoba, D., 2002. Rainfall variability in West Africa during the years 1950–1990. J. Clim. 15, 187–202.

Mayaux, P., De Grandi, G.F., Rauste, Y., Simard, M., Saatchi, S., 2002. Large scale vegetation maps derived from the combined L-band GRFM and C-band CAMP wide area radar mosaics of Central Africa. Int. J. Remote Sens. 23, 1261–1282.

Mougin, E., Lopes, A., Frison, P.L., Proisy, C., 1995. Preliminary analysis of ERS-1 wind scatterometer data over land surfaces. Int. J. Remote Sens. 6, 391–398.

Mougin, E., Hiernaux, P., Kergoat, L., de Rosnay, P., Grippa, M., Timouk, F., Arjounin, M., Le Dantec, V., Demarez, V., Ceschia, E., Mougenot, B., Baup, F., Frappart, F., Frison, P.-L., Gardelle, J., Gruhier, C., Jarlan, L., Mangiarotti, S., Sanou, B., Tracol, Y., Guichard, F., Trichon, V., Diarra, L., Soumaré, A., Koité, M., Dembélé, F., Lloyd, C., Hanan, N.P., Damesin, C., Delon, C., Serça, D., Galy-Lacaux, C., Seghiéri, J., Becerra, S., Dia, H., Gangneron, F., Mazzega, P., 2009. The AMMA-CATCH Gourma observatory site in Mali: relating climate variations to changes in vegetation, surface hydrology, fluxes and natural resources. J. Hydrol. 375 (1–2), 14–33.

Naeimi, V., Scipal, K., Bartalis, Z., Hasenauer, S., Wagner, W., 2009. An improved soil moisture retrieval algorithm for ERS and METOP scatterometer observations. IEEE Trans. Geosci. Remote Sens. 47 (7), 1999–2013.

Nashashibi, A.Y., Sarabandi, K., Oveisgharan, S., Dobson, M.C., Walker, W.S., Burke, E., 2004. Millimeter-wave measurements of foliage attenuation and ground reflectivity of tree stands at nadir incidence. IEEE Trans. Antenn. Propag. 52 (5), 1211–1222.

Nicholson, S.E., 1980. The nature of rainfall fluctuations in subtropical West-Africa. Mon. Weather Rev. 109, 2191–2208.

Owe, M., De Jeu, R.A.M., Holmes, T.R.H., 2008. Multi-sensor historical climatology of satellite-derived global land surface moisture. J. Geophys. Res. 113, F01002.

Papa, F., Legresy, B., Remy, F., 2003. Use of the Topex-Poseidon dual-frequency radar altimeter over land surfaces. Remote Sens. Environ. 87, 136–147.

Prigent, C., Aires, F., Jimenez, C., Papa, F., Roger, J., 2014. Multiangle backscattering observations of continental surfaces in Ku-Band (13 GHz) from satellites: understanding the signals, particularly in arid regions. IEEE Trans. Geosci. Remote Sens. 53 (3), 1364–1373.

Ridley, J., Strawbridge, F., Card, R., Phillips, H., 1996. Radar backscatter characteristics of a desert surface. Remote Sens. Environ. 57 (2), 63–78.

Rosenqvist, Å., Birkett, C.M., 2002. Evaluation of JERS-1 SAR mosaics for hydrological applications in the Congo river basin. Int. J. Remote Sens. 23 (7), 1283–1302.

Santos Da Silva, J., Seyler, F., Calmant, S., Rotunno Filho, O.C., Roux, E., Araújo, A.A.M., Guyot, J.-L., 2012. Water level dynamics of Amazon wetlands at the watershed scale by satellite altimetry. Int. J. Remote Sens. 33 (11), 3323–3353.

Santos Da Silva, J., Calmant, S., Seyler, F., Corrêa Rotunno Filho, O., Cochonneau, G., Mansur, W.J., 2010. Water levels in the Amazon basin derived from the ERS 2 and ENVISAT radar altimetry missions. Remote Sens. Environ. 114, 2160–2181.

Schneider, U., Becker, A., Meyer-Christoffer, A., Ziese, M., Rudolf, B., 2011. Global Precipitation Analysis Products of the GPCC. Global Precipitation Climatology Centre (GPCC), DWD, Internet Publication, pp. 1–13, <http://www.dwd.de/bvbw/appmanager/bvbw/dwdwwwDesktop?_nfpb=true&_pageLabel=_dwdwww_klima_umwelt_datenzentren_wzn&T12404918261141645319968gsbDocumentPath=Content%2FOeffentlichkeit%2FKU%2FKU4%2FKU42%2Fen%2FReports__Publications%2FGPCC__intro__products__2011.html>.

Simard, M., De Grandi, F., Saatchi, S., Mayaux, P., 2001. Mapping tropical coastal vegetation using JERS-1 and ERS-1 radar data with a decision tree classifier. Int. J. Remote Sens. 23, 1461–1474.

Stephen, H., Long, D., 2005. Microwave backscatter modeling of Erg surfaces in the Sahara desert. IEEE Trans. Geosci. Remote Sens. 43 (2), 238–247.

Stephen, H., Long, D., 2007. Spatial and temporal behavior of microwave backscatter directional modulation over the Saharan Ergs. IEEE Trans. Geosci. Remote Sens. 45 (5), 1164–1173.

Ulaby, F.T., Moore, R.K., Fung, A.K., 1982. Microwave remote sensing: Active and passive. Radar Remote Sensing and Surface Scattering and Emission, vol. 2. Artech House, Norwood, MA.

Ulaby, F.T., Moore, R.K., Fung, A.K., 1986. Microwave remote sensing: Active and passive. From Theory to Applications, vol. 3. Artech House, Norwood, MA.

Van De Giesen, N., 2001. Characterization of West African shallow flood plains with L-and C-Band radar. In: Owe, M., Brubaker, K. (Eds.), Remote Sensing and Hydrology 2000 (67). IAHS Publication, Paris, France, pp. 365–367.

Verron, J., Sengenes, P., Lambin, J., Noubel, J., Steunou, N., Guillot, A., Picot, N., Coutin-Faye, S., Gairola, R., Raghava Murthy, D.V.A., Richman, J., Griffin, D., Pascual, A., Rémy, F., Gupta, P.K., in press. The SARAL/AltiKa altimetry satellite mission. Mar. Geodesy.

Vincent, P., Steunou, N., Caubet, E., Phalippou, L., Rey, L., Thouvenot, E., Verron, J., 2006. AltiKa: a Ka-band altimetry payload and system for operational altimetry during the GMES period. Sensors 6, 208–234.

Wagner, W., Lemoine, G., Rott, H., 1999a. A method for estimating soil moisture from ERS scatterometer and soil data. Remote Sens. Environ. 70 (2), 191–207.

Wagner, W., Lemoine, G., Borgeaud, M., Rott, H., 1999b. A study of vegetation cover effects on ERS scatterometer data. IEEE Trans. Geosci. Remote Sens. 37 (2), 938–948.

Waite, W.P., MacDonald, H.C., 1971. "Vegetation penetration" with K-band radars. IEEE Trans. Geosci. Remote Sens. GE-9 (3), 147–155.

Wigneron, J.P., Kerr, Y., Waldteufel, P., Saleh, K., Escorihuela, M.J., Richaume, P., et al., 2007. L-band microwave emission of the biosphere (L-MEB) model: description and calibration against experimental data sets over crop fields. Remote Sens. Environ. 107, 639–655.

Wingham, D.J., Rapley, C.G., Griffiths, H., 1986. New techniques in satellite altimeter tracking systems. In: Proc. IGARSS'86 Symposium, Zürich, 8–11 September 1986. ESA SP-254, pp. 1339–1344.

Woodhouse, I.H., Hoekman, D.H., 2000. Determining land-surface parameters from the ERS wind scatterometer. IEEE Trans. Geosci. Remote Sens. 38 (1), 126–140.

Zelli, C., 1999. ENVISAT RA-2 advanced radar altimeter: instrument design and pre-launch performance assessment review. Acta Astronaut. 44 (7), 323–333.

Zribi, M., Saux-Picart, S., André, C., Descroix, L., Ottlé, O., Kallel, A., 2006. Soil moisture mapping based on ARSAR/ENVISAT radar data over a Sahelian site. Int. J. Remote Sens. 28 (16), 3547–3565.

Zribi, M., Pardé, M., de Rosnay, P., Baup, F., Boulain, N., Descroix, L., Pellarin, T., Mougin, E., Ottle, C., Decharme, B., 2009. ERS scatterometer surface soil moisture analysis of two sites in the south and north of the Sahel region of West Africa. J. Hydrol. 375 (1–2), 253–261.

Zwarts, L., Grigoras, I., 2005. Flooding of the Inner Niger Delta. In: Zwarts, L., Beukering van, P., Kone, B., Wymenga, E. (Eds.), The Niger, A Lifeline. RIZA/Wetlands International/IVM/A&W, Lelystad, pp. 43–77.